International Journal of Basic and Applied Sciences, 14 (4) (2025) 462-474

International Journal of Basic and Applied Sciences

Website: www.sciencepubco.com/index.php/IJBAS
https://doi.org/10.14419/g10zn898
Research paper

A Novel Multi-Sensor Fusion SLAM Framework for Anti-Interference

Yu Ji *, Jian Qu

School of Engineering and Technology, Panyapiwat Institute of Management, Nonthaburi,11120, Thailand
**Corresponding author E-mail: jianqu@pim.ac.th*

Received: July 31, 2025, Accepted: August 7, 2025, Published: August 16, 2025

Abstract

Nowadays, people have high requirements for the robustness of autonomous driving. As a key technology in the field of autonomous driving, SLAM requires a lightweight and explainable algorithm framework when dealing with perception degradation scenes. At present, most multi-sensor fusion SLAM algorithms use methods such as training neural networks or adding new odometry constraints to achieve anti-interference, but these methods do not meet the requirements. We use the data communication technology of the ROS (Robot Operating System) platform to integrate the CLAHE (Contrast Limited Adaptive Histogram Equalization) algorithm, the LiDAR Noise Filtering algorithm, and RTAB-Map (a multi-sensor fusion algorithm based on graph optimization). We then conducted experiments in three designed perception degradation scenes and used the MME indicator to quantify the experiments. The results showed that the MME of our framework in the perception-degraded environment was reduced by an average of 0.107, proving that the framework we proposed performs bet-ter than RTAB-Map in dealing with some perception degradation scenes.

Keywords: *Multi-Sensor Fusion; ROS; SLAM; CLAHE Algorithm; LiDAR Noise Filtering.*

1. Introduction

1.1. Research background and significance

SLAM (Simultaneous Localization and Mapping) [1] technology is widely used in the field of autonomous driving. Among them, multi-sensor fusion solutions (vision, LiDAR, IMU (Inertial Measurement Unit), wheel odometry, etc.) [2–4] have gradually become the mainstream trend to improve robustness in complex environments due to their perception redundancy and data complementarity. RTAB-Map (Real-time appearance-based mapping) is a graph-optimized SLAM system [5–7] that supports multiple sensor inputs and is widely used in indoor and outdoor mapping tasks.

Although the multi-sensor fusion SLAM system has perception redundancy, it is still susceptible to interference from sensor data sources with degraded perception. For example, interference from data sources such as insufficient light, texture loss, and LiDAR noise will directly increase positioning errors and reduce mapping accuracy. Most researchers focus on backend optimization and algorithm improvement, while there is little research on the anti-interference of sensor data source quality in multi-sensor fusion SLAM, which limits the stability and adaptability of SLAM systems in actual complex environments.

Therefore, it is of great research value to improve the anti-interference ability of data sources in multi-sensor fusion SLAM systems.

1.2. Classification of perceptual degradation

In real-world applications, SLAM systems are often in non-ideal environments, and the quality of data sources is susceptible to interference. A degraded environment will reduce the quality of sensor data and thus reduce the robustness of mapping. We divide perception degradation types into visual perception degradation and LiDAR perception degradation according to the type of external sensor.

1.2.1. Degradation of visual perception

In low-light environments such as at night, in tunnels, or underground garages, Images are usually low in brightness and poor in contrast, which results in sparse or even missing image feature points. In scenes with simple structures and a lack of obvious texture information, such as white walls or open areas, the image content lacks local texture features, resulting in sparse image feature points.

These two common camera perception degradations directly lead to the failure of image matching between frames of the visual odometry, reducing the success rate of loop detection and thus weakening the mapping accuracy of the entire SLAM system.

In 2017, Yang et al. [8] pointed out that point-feature-based visual SLAM (such as ORB-SLAM and LSD-SLAM) performs extremely poorly in scenes with sparse textures. The number of obtainable feature points is significantly reduced, thereby reducing the accuracy of mapping. In 2017, Pire et al. [9] demonstrated through quantitative analysis that in low-light scenes, a decrease in the number of ORB feature points of more than 60% would result in a 3-fold increase in the tracking loss rate. The experiment proved that low-light environments would seriously reduce the ability of SLAM visual odometry to extract feature points.

1.2.3. LiDAR perception degradation

In a single-structure environment such as a long straight corridor or an empty room, the LiDAR data lacks significant geometric changes, resulting in insufficient spatial features required for loop detection and weakened matching constraints of the laser odometry. This perception degradation leads to laser noise or mismatches between local maps, which seriously reduce the mapping accuracy of the SLAM system. In 2020, Shan et al. [10] confirmed that in an empty warehouse, the translation error of the laser odometry far exceeds that in a structured scene. They demonstrated that the lack of spatial features in the LiDAR point cloud will cause mismatches between local maps. In 2024, Tuna et al. [11] specifically pointed out in their paper that in degenerative environments, such as long corridors, the performance of traditional laser odometry based on point-to-point or point-to-surface measurements will deteriorate significantly.

1.3. Objectives and technical route

In order to improve the mapping accuracy of the SLAM system in a perception-degraded environment, this paper proposes a multi-sensor fusion SLAM framework based on data source anti-interference. We introduce a lightweight perception module to enhance the anti-interference ability of the sensor data source, and then input the enhanced sensor data into RTAB-Map and output a 3D map. Our framework can improve the robustness of the system and enhance the anti-interference ability of sensor data in a perception-degraded environment. In terms of specific operations, we referred to and improved the methods proposed by NTNU Autonomous Robots Lab and the GitHub project released by George Chrysanthidis [12, 13]. Our framework does not modify the RTAB-Map algorithm, but only performs anti-interference processing on the data input end. The system design of this paper consists of the following two core parts.

1.3.1. Visual image enhancement module

In 2022, Yu et al. [14] proposed AFE-ORB-SLAM, an ORB-SLAM algorithm based on adaptive FAST threshold and image enhancement, which is suitable for low-light environments. The improved automatic gamma correction is combined with unsharp masking. Experimental results show that AFE-ORB-SLAM can achieve high positioning and mapping accuracy under low-light conditions. In 2024, Lin et al. [15] proposed a visual SLAM enhancement algorithm that combines CLAHE with AGCWD (Adaptive Gamma Correction with Weighting Distribution) to improve the brightness and contrast of underground space visual images. Experiments show that the method proposed by Lin et al. reduces the RMSE (root mean square error) of the trajectory to 0.17m, which is a significant improvement.
The article by Yu and Lin et al. demonstrated the feasibility of combining the CLAHE algorithm with the SLAM system, which provided the basis for our research. However, we use the CLAHE algorithm to enhance the anti-interference ability of the multi-sensor fusion framework. This is not common in the scientific research community and is the innovation of our work.
We employ the CLAHE algorithm [16] to perform real-time preprocessing of camera images. It can enhance the local contrast of images in environments with insufficient lighting and a lack of texture, improve the success rate of feature point extraction in images, and enhance the robustness and constraint of visual odometry.

1.3.2. LiDAR noise filtering module

In 2021, Frosi et al. [17] proposed a real-time laser SLAM system. The front-end uses a distance filtering method to remove LiDAR noise beyond the distance range, thereby significantly improving the robustness of pose estimation and mapping accuracy. Experiments show that the effect is better than that of the LOAM and LeGO-LOAM algorithms. In 2024, Ferrari et al. [18] proposed a point cloud filtering method based on median deviation and distance threshold to improve the robustness of LiDAR-SLAM in noisy scenes, and used public datasets for verification, proving that this method can improve the robustness of pose estimation and the accuracy of mapping.
The article by Frosi and Ferrari et al. provides the basis for combining range filters, Median Deviation, and ROS systems. We use the LiDAR denoising module to enhance the multi-sensor fusion SLAM data source and give it anti-interference capabilities. This practice is not common in the scientific research community.
We combine the range filter with the median deviation algorithm to filter the input 2D LiDAR data. By removing distant and abnormal LiDAR noise in the real environment, the robustness and constraint of the laser odometry in the perception-degraded environment are improved.

1.4. Popular multi-sensor fusion and anti-interference methods

Multi-sensor fusion refers to the combination of multiple heterogeneous or homogeneous sensor data for timestamp alignment and TF (Transform) coordinate alignment for subsequent algorithm use.
In 2013, Li et al. [19] proposed the MSCKF2.0 scheme based on the loosely coupled framework of CKF-MSS (Constrained Kalman Filter with Multiple States), using IMU pre-integration to compensate for visual odometry degradation. In 2019, Labbé et al. [6] proposed the multi-sensor fusion algorithm RTAB-MAP based on graph optimization, which can fuse sensor data such as RGB-D (Red-Green-Blue and Depth), LiDAR, and IMU, and proposed hierarchical memory management to deal with the risk of memory explosion. In 2022, Lin et al. [20] proposed the R3LIVE scheme based on IEKF (Iterated Extended Kalman Filter), which uses the joint estimation of LiDAR, IMU, and RGB-D to improve robustness.
However, each sensor has advantages and disadvantages. When we combine the advantages of sensors, their disadvantages are also combined. Therefore, the perception-degraded environment will weaken most of the existing multi-sensor fusion frameworks. Therefore, scholars in the research community have proposed methods such as training anti-interference models of neural networks and adding new sensor constraints. However, these methods lack lightweight capabilities and impose additional computational burdens on autonomous driving systems. Furthermore, Methods based on training neural networks require significant human resources and time for data collection and model training, resulting in poor timeliness.

In 2021, Jia et al. [21] proposed a tightly coupled multi-sensor fusion algorithm, Lvio-Fusion SLAM, which uses reinforcement learning methods to adaptively adjust the weights of each sensor. Experimental results show that Lvio-Fusion SLAM can achieve robust pose estimation and mapping in an environment with degraded perception. In 2024, Lee et al. [22] proposed a switch-based LiDAR-Visual-Inertial SLAM-Switch-SLAM, which aims to solve the anti-interference problem in a perception-degraded environment. When the laser odometry is detected to be degraded, the switch structure disables the laser odometry and relies on the visual odometry to achieve robust pose estimation and mapping. In 2025, Li et al. [23] proposed a sensor adaptive compensation strategy based on deep learning. Through the trained lightweight network model, the degree of sensor degradation is detected in real time, and different weights are assigned to each sensor according to the degree of degradation. Through experiments, Li et al. proved that the improved SLAM has anti-interference ability in a sensor-degraded environment.

1.5. Contributions

A multi-sensor fusion SLAM framework with anti-interference ability based on graph optimization is proposed to avoid intrusive modification of the original algorithm.
Build an explainable perceptual degradation response mechanism and design corresponding data enhancement modules for the noise interference of RGB-D and LiDAR.
We used a physical smart car to conduct field tests, selecting typical perception degradation scenes such as low-light environments, sparse image texture environments, open spaces, and long corridors.
Because the acquisition and comparison of ground truth are controversial, we introduce a fair comparison framework, MapEval [24], without using controversial ground truth values. The MME (Mean Map Entropy) indicator is introduced to evaluate the output 3D point cloud map, realizing quantitative analysis and validity verification without reference to ground truth values.

2. Materials and methods

2.1. Smart car hardware introduction

The smart car [25, 26] is equipped with Ubuntu 20.04; ROS-Foxy operating system, and its sensor is equipped with ORBBEC 's Astra pro plus model RGB-D camera, SLAMTEC A1 model 2D LiDAR, 9-axis IMU, and wheel odometry, the processor is Jetson Orin Nano, and the driver board uses ROS expansion board. In addition, for the convenience of actual operation and to meet the needs of the experiment, we added a USB UHB expansion board, an Ackerman baseboard, and a touch screen. As shown in Figure 1 and Table 1, we can see the structure, software, and hardware configuration of the smart car.

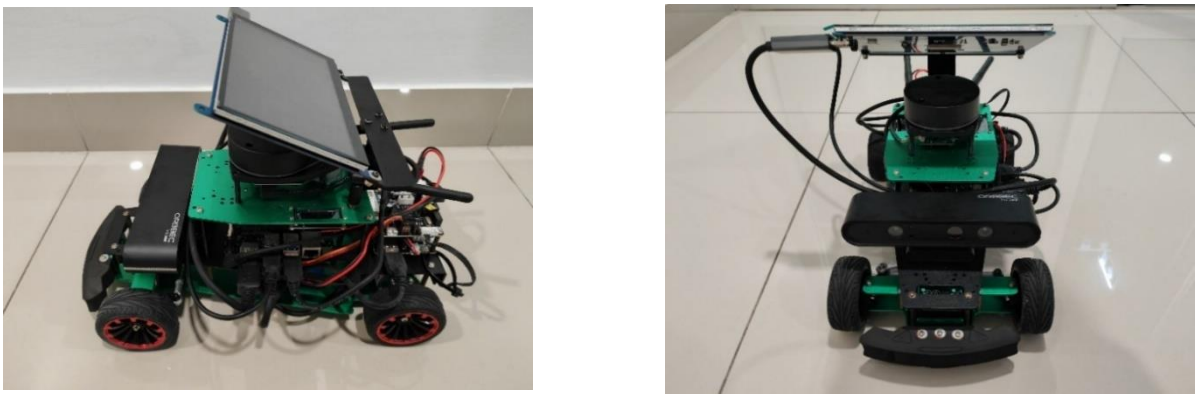

Fig. 1: Smart Car Structure.

Table 1: Smart Car Hardware and Software Configuration

Classification	Detailed
Operating System	ROS2 Foxy
Sensor	RGB-D Camera
	2D LiDAR
	9-axis IMU
	Wheel Odometry
GPU	Jeston Orin Nano
Expansion Board	ROS Expansion Board
	USB UHB Expansion Board
Base Plate	Ackerman baseboard
Operation board	Touch Screen

2.2. System overall framework

Our framework is divided into two parts, namely the front-end sensor data source anti-interference module and the back-end multi-sensor fusion SLAM algorithm module (RTAB-MAP). The data structure of the RTAB-Map system is developed around the joint input of vision, LiDAR, IMU, and wheel odometry, and the node connection is realized through the topic communication mechanism of ROS (Robot Operating System). We draw the sensor data processing flow of our framework, as shown in Figure 2.

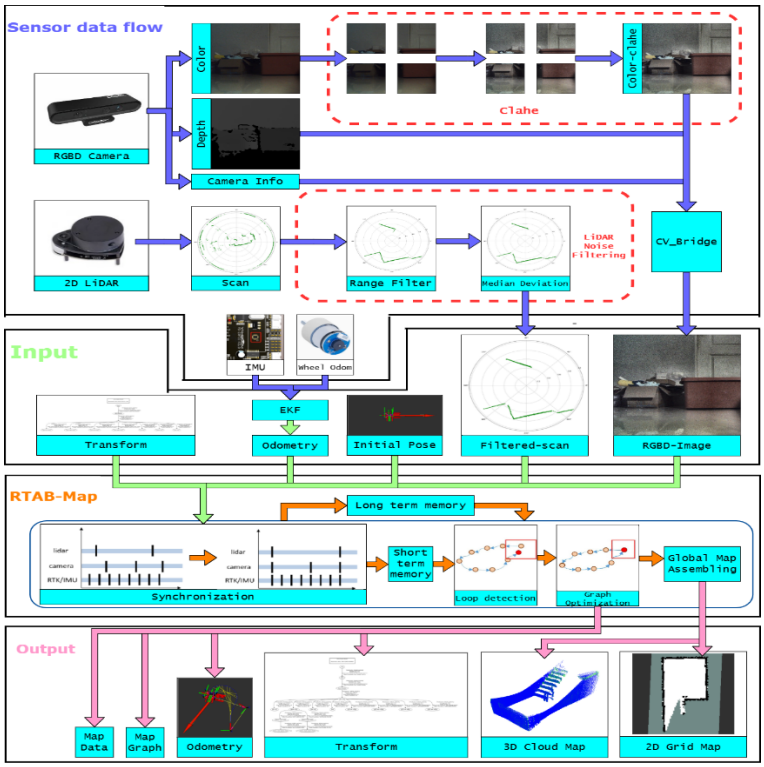

Fig. 2: Our Framework Data Flow.

2.2.1. RGB-D camera data flow

The RGB-D camera publishes three topics through ROS 2 [27]: original color image, depth image, and camera intrinsics. Among them, the CLAHE visual enhancement module subscribes to the original color image topic, applies the contrast-limited adaptive histogram equalization algorithm to improve the image quality, and replaces the original color image topic with the enhanced color image. The RGBD-sync node subscribes to the following topics: 1. Color image enhanced by the CLAHE module, 2. Depth image, 3. Camera intrinsics. The node synchronizes the timestamps and aligns the spatial TF for the three subscribed topics [28], fuses the data of the three topics, generates encapsulated RGBD-Image data, and then inputs the RGBD-Image data into the RTAB-Map algorithm.

Key note: The color image in the RGBD-Image is the result of the enhancement by the CLAHE module, and the depth map and intrinsics maintain the original input; the message type and structure remain unchanged, only the color image content is enhanced, and there is no need to realign the timestamp or correct the TF.

2.2.2. LiDAR data flow

The 2D LiDAR publishes the original topic. The LiDAR Noise Filtering module subscribes to the original LiDAR topic and then publishes a new topic after the LiDAR noise is removed by the range filter and median deviation algorithm. We use the ROS2 topic communication mechanism [29, 30] to ensure that the message type of the data in the topic before and after processing remains unchanged. We only replace the original LiDAR topic with the processed new topic, so there is no need to realign the timestamps between multi-sensor data or correct TF.

2.2.3. IMU and wheel odometry data flow

The IMU (inertial measurement unit) and wheel odometry integrated in the system publish their sensor data topics respectively, and rely on the EKF (Extended Kalman Filter) node. This node filters and fuses the IMU and wheel odometry data, and outputs the odometry message in a unified format, which is published to the odometry. The odometry data is used as a pose before providing a more accurate and robust initial pose estimation for the subsequent SLAM system or positioning module.

2.2.4. RTAB-Map main processing flow

Although the original RTAB-Map is highly modular, it is highly sensitive to the quality of sensor input, especially in perception degradation scenes, where anomalies in image and radar data will directly affect the accuracy of mapping and trajectory stability. Therefore, this study proposes an input enhancement strategy based on this to improve the robustness of the system in complex scenes.

Finally, our framework subscribes to the following sensor topics: 1. RGBD-Image; 2. Processed LiDAR topic; 3. Odometry after EKF fusion; 4. Initial pose provided by the vehicle base: Initialpose; 5. TF containing the coordinates of each sensor.

Through the front-end visual/laser odometry node and the back-end graph optimization module, our framework can publish the following main topics in real time: 1. Map Data; 2. Map Graph; 3. Corrected odometer; 4. TF: coordinate transformation between each sensor and the map and base; 5. 2D grid map; 6. 3D point cloud map.

2.3. Visual CLAHE enhancement module

To improve the robustness of a visual odometry in a visual perception degradation environment, we designed a visual CLAHE enhancement module. This module is implemented in the form of a ROS 2 node, which subscribes to the original color image topic in real time, and the processing flow and engineering implementation are as follows:

2.3.1. Processing flow

The depth camera image is first converted to an OpenCV image through CV_Bridge [31]. Then the BGR image (RGB and BGR differ only in order) is converted to the Lab color space, and the brightness channel (L) is separated, and then the L channel in the Lab image is subjected to local contrast enhancement. CLAHE uses two parameters, block size and clip limit, to perform histogram equalization on each image block. The enhanced L channel is merged with the original a and b channels. The Lab image is converted back to a BGR image. The merged image is transferred back to ROS through cv_bridge for use by the algorithm.
The CLAHE algorithm divides the image into several blocks, performs histogram equalization on each local area independently, and uses the clip limit threshold to control noise anomalies. The formula is as follows:

$$T(i) = \frac{L-1}{M \times N} \sum_{j=0}^{i} h_c(j) \quad (1)$$

Where T(i) is the mapping of gray level i; L is the total number of gray levels (usually 256); M×N is the number of pixels per grid block in the image; and $h_c(j)$ is the pixel count of gray level j after cropping.
The specific enhancement parameters are as follows: Tile size (tileGridSize): can be adjusted dynamically, the default setting is 8×8, taking into account both local details and computational efficiency. The larger the tileGridSize, the clearer the local details, but the lower the computational efficiency and the heavier the system burden; Contrast limit (clipLimit): can be adjusted dynamically; the default setting is 4.0, effectively suppressing noise anomalies. High values will increase the contrast of irrelevant objects, increasing the computational burden, but low values will have little effect.

2.3.2. Topic output and ROS 2 interface

The image data enhanced by the CLAHE visual enhancement module is repackaged into the sensor_msgs/msg/RGBD-Image format and updated in real time to maintain compatibility with other module interfaces in the system, facilitating the use of the subsequent RTAB-Map algorithm.

2.3.3. Engineering implementation

We use OpenCV 4.5 and ROS 2 rclpy Python framework development, and use cv_bridge to realize ROS image data and OpenCV data conversion; support ROS 2 dynamic parameter server, the system can adjust clipLimit and gridSize in real time during operation, which is convenient for adapting to different environments; introduce an exception feedback mechanism to ensure that the ROS main process is not interrupted when the image processing is abnormal; the topic interface is fully compatible with the RTAB-Map module and can be integrated into the overall SLAM process of the system.

2.4. LiDAR noise filtering module

Given the common noise in LiDAR data, this system has designed a LiDAR denoising module. This module includes a range filter and a median deviation algorithm, which effectively improves the anti-interference ability of LiDAR while ensuring real-time performance.

2.4.1. Range filter

First, the input LiDAR data is roughly screened to remove LiDAR point clouds that are beyond the effective working range. By setting the minimum and maximum distance thresholds, the physical error data can be reduced. We set the minimum value to exclude abnormal point clouds caused by physical structures such as the smart car bracket, and set the maximum value to remove distant noise that is irrelevant to the scene. The formula is as follows:

$$d_{min} < d_i < d_{max}, i \in [1, N] \quad (2)$$

Among them, d_i is the distance measurement value of the i-th laser echo, and N is the total number of laser beams in the current frame. In actual applications, the minimum value of the range filter is taken from the laser radar equipment parameters (to offset the influence of the system itself such as the smart car bracket), and the maximum value of the range filter is set to 3.0 m, mainly for the close-range mapping scene of this system, to eliminate long-range weak echoes and noise in advance.

2.4.2. Median deviation filter

On the basis of range screening, the local sliding window median deviation algorithm is further used to suppress local abnormal noise. The specific steps are as follows: the distance data is processed in segments with a fixed window length, and the median is calculated for each window. If any laser beam distance measurement value d_i meets the requirements of the following formula, the value is judged as abnormal, and a special mark value (such as 10m) is assigned for subsequent system processing. The formula is as follows:

$$\frac{med-elem}{med} \times 100 > 20\% \quad (3)$$

Where med is the median of the laser radar distance value in this interval, and elem is a laser ranging value in the current interval. The value is considered abnormal, and a special mark value (such as 10m) is assigned for subsequent system processing.
Experiments show that this method has good robustness when dealing with single-structure environments such as long corridors and empty rooms.

2.4.3. Topic output and ROS 2 interface

The LiDAR data, enhanced by the range filter and median deviation algorithm, is repackaged into the sensor_msgs/msg/LaserScan format and published to a new topic in real time to maintain compatibility with other module interfaces of the system and facilitate the use of the subsequent RTAB-Map algorithm.

2.4.4. Engineering implementation

We developed the client library based on ROS 2 rclpy Python. Tested on the Jetson Orin Nano platform, the average delay of laser data processing is less than 5 ms. It supports module anomaly detection, which can effectively improve the robustness of noise removal in a sensory degradation environment. The whole process follows the ROS 2 message format standard, only modifying the RTAB-Map subscription topic, without modifying the internal algorithm.

2.5. Integration with RTAB-Map

The RTAB-Map algorithm will automatically subscribe to the default sensor data (original color image topic, etc.). However, when we use the CLAHE module and the LiDAR Noise Filtering module to process the original topic and publish a new topic, the original topic and the new topic will coexist. The new topic data depends on the original topic, so we cannot delete the original topic data. Therefore, we use the ROS remapping mechanism to achieve seamless integration of our anti-interference system and RTAB-Map: 1. The remapped image topic is a new topic published after enhancement by the CLAHE module; 2. The remapped laser topic is a new topic published after enhancement by the LiDAR Noise Filtering module 3. The subscription name of the odometry after the fusion of the IMU and the wheel odometry remains unchanged; 4. We only modify the topic name subscribed in the RGBD-sync module in the RTAB-Map algorithm and the topic name subscribed in the remapping launch file, and do not make major changes to the internal structure of the algorithm.

2.6. Experimental objectives

This section aims to verify the effect of our proposed sensor data source anti-interference module (CLAHE and LiDAR Noise Filtering) on the mapping accuracy improvement of the RTAB-Map system in a perception-degraded environment.
The specific experimental objectives include: 1. Compare the mapping accuracy of the system before and after enhancement in three perceptual degradation scenes [32]; 2. Quantitatively analyze the 3D point cloud map to verify the anti-interference ability of our method; 3. Prove that this method can still significantly improve system performance without changing the internal core algorithm of RTAB-Map, and has good engineering practicality.

2.7. Experimental scene design

This chapter selects three classic perceptual degradation scenes for field verification [33]. The perceptual degradation types include sparse image texture, insufficient light, and insufficient laser spatial features. To enhance readers' spatial perception of our three experimental scenes, we have added schematic diagrams of the scenes and 2D grid maps of the three experimental scenes below.

2.7.1. Sparsely textured and empty rooms

Scene 1 is an empty elevator room with sparse textures. There is a white wall and a glass wall without any texture. The room is empty, with no other recognizable objects except the walls, doors, and windows, and the LiDAR spatial features are insufficient. When the smart car is driving in an empty room, the camera cannot provide enough corner points, thus weakening the image constraints, and feature point matching failures may occur, resulting in map drift. As shown in Figure 3, we can see the schematic diagram of scene 1 and the 2D grid map.

Fig. 3: (A) Schematic Diagram of Scene 1. (B) 2D Grid Map of Scene 1.

2.7.2. Sparsely textured and long corridors

Scene 2 is a long corridor with sparse textures. The corridor is flanked by large white walls and doors with repeated structures. The overall lack of rich image texture information makes it difficult for the camera to stably extract enough feature points. The space is long and deep, and the point cloud of the LiDAR at the limit of the filtering range will have a large deviation. In addition, due to the highly symmetrical and repetitive structure of the corridor, it is easy for the visual and LiDAR data to fail to match when building the map, thereby reducing the success rate of loop detection and even causing local map mismatching problems, which seriously reduces the robustness of the system. As shown in Figure 4, we can see the schematic diagram of scene 2 and the 2D grid map.

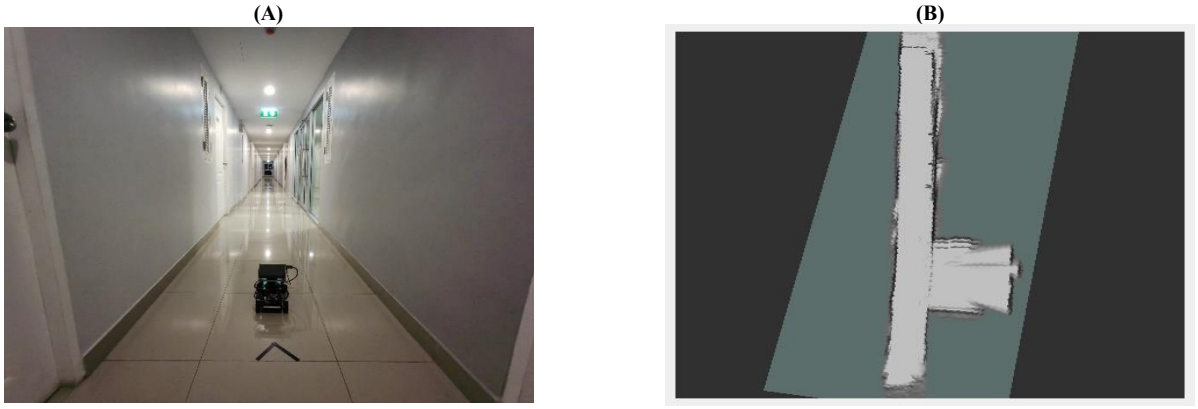

Fig. 4: (A) Schematic Diagram of Scene 2. (B) 2D Grid Map of Scene 2.

2.7.3. Sparsely textured and dimly lit stairwell

Scene 3 is an elevator room with insufficient light. The white walls in the elevator room have sparse textures. The images collected by the visual sensor in this environment have low brightness and weak contrast. The number of effective feature points in the image is significantly reduced, and the robustness is poor. It is very easy to cause the intelligent vehicle to drift, thereby reducing the accuracy and robustness of the map. As shown in Figure 5, we can see the schematic diagram of scene 3 and the 2D grid map.

The light in scene 3 is too dim, and it is difficult to see the details of the picture. We perform exposure processing on scene 3. As shown in Figure 5, there is a schematic diagram of scene 3, a schematic diagram of scene 3 after exposure, and a two-dimensional grid map of scene 3.

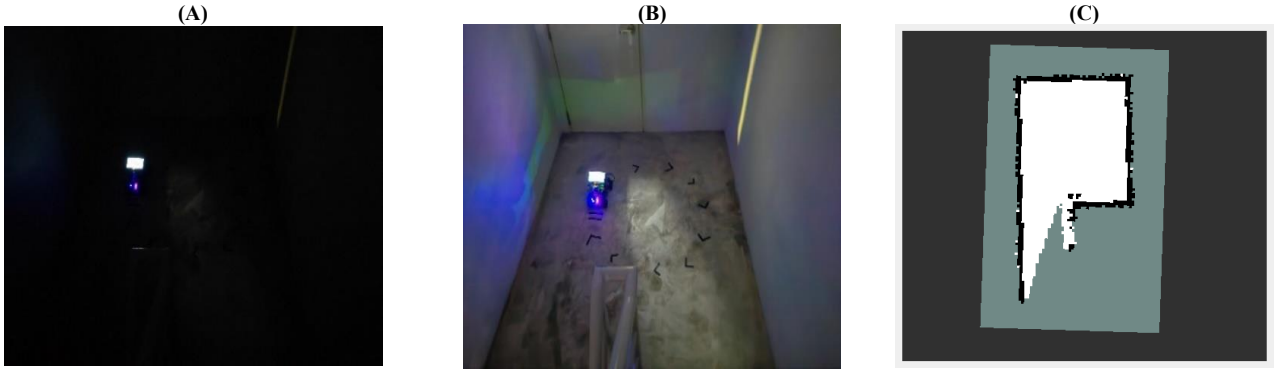

Fig. 5: (A) Schematic Diagram of Scene 3. (B) Schematic Diagram of Scene 3 After Exposure. (C) 2D Grid Map of Scene 3.

2.8. Data processing principles

We use smart cars to avoid external influences and human errors when building maps in reality [25, 32]. To ensure the fairness and reproducibility of the experiment, all experiments are based on a unified platform, sensor configuration, and data processing flow. We run the RTAB-Map system in two modes: turning on and off the enhancement module. When building a 3D point cloud map, ensure that it is completed within the same period, and the smart car drives along the designed fixed route.

2.9. Evaluation metrics and visualization methods

We choose MapEval [24] as the evaluation framework, MME as the evaluation indicator for quantitative analysis, and the error map as the evaluation basis for qualitative analysis. The following are the details

2.9.1. Reasons for selection

The opacity of ground truth acquisition makes this reference indicator controversial when comparing SLAM results. Ground truth is a good reference indicator in simulation environments. But in real environments, because a completely accurate ground truth is difficult to obtain and very easy to forge, we do not use ground truth as a reference indicator in our experiments.

The technical threshold and cost of deploying high-precision external measurement instruments (such as total stations and laser ranging arrays) in complex environments are high, and it is difficult to obtain reference ground truth for SLAM result data comparison.

To solve the above problems, we use MapEval, a SLAM evaluation framework that does not require ground truth, jointly proposed by the Hong Kong University of Science and Technology, City University of Hong Kong, and the University of Science and Technology Beijing in 2025. This framework is used to solve the problem of SLAM evaluation without an expensive ground truth reference, and proposes a unified, universal, and external positioning system-free mapping quality evaluation method, which has been applied and verified in multiple SLAM research scenarios without ground truth.

MapEval outputs the MME (Mean Map Entropy) of the map point cloud through a statistical system, which fully reflects the consistency and chaos of the 3D point cloud map. The smaller the MME value, the higher the consistency of the 3D point cloud map, the lower the chaos, and the better the mapping effect. At the same time, MapEval can also output an error map for qualitative analysis of the degree of drift of the 3D point cloud map. The more irregular the 3D point cloud map is, the higher the degree of chaos it represents.

2.9.2. Operation notes

Before using MapEval to calculate the MME, we use CloudCompare to unify the scale of the 3D point cloud images to be compared and align their coordinate systems. Then modify the config file to ensure that the similarity of the two 3D point cloud images to be compared is above 99.5%.

2.9.3. Summary

In order to avoid controversy and suspicion of fraud caused by using ground truth, we use the MME indicator for reference. Based on the MapEval framework, this paper uses MME as the core performance indicator for quantitative analysis to conduct a unified quantitative analysis of the system's mapping accuracy in common perception degradation environments. This indicator is suitable for scenarios without ground truth reference and can reflect the robustness of the SLAM system in a perception-degraded environment. At the same time, we use the output raw error map and the inlier error map for qualitative analysis [24].

3. Results and discussion

In order to evaluate the effect of the proposed anti-interference multi-sensor fusion SLAM system in perception degradation scenes, we designed a systematic comparative experiment containing three classic perception degradation scenes. To avoid controversy and suspicion of fraud caused by using ground truth. We use the MME indicator in the MapEval evaluation framework for quantitative analysis and combine the error map for qualitative verification.

3.1. MME indicator description

MME (Mean Map Entropy) is an entropy value. The smaller the MME value (for example, -9 corresponds to a better effect than 8), the lower the confusion of the 3D point cloud map and the closer it is to the ideal state (the theoretical minimum value is -10 and the maximum value is 0) [24].
To give reviewers a more intuitive understanding of the MME indicator. We cite two papers that use the MME indicator to evaluate the robustness of the SLAM system: In 2024, Hu et al. [34] published an article in the IEEE Robotics & Automation Society, mentioning the PAloc algorithm and FL2 (FAST-LIO2) algorithm. They used the MME indicator to conduct 6 sets of comparative experiments in different scenes. The MME entropy value dropped by an average of 0.095. As shown in Table 2, we can see the specific MME data of Hu et al. The data address: https://github.com/JokerJohn/Cloud_Map_Evaluation?tab=readme-ov-file [24].

Table 2: Specific MME Data of Hu et al

Metrics	Alg.	Scene 0	Scene 2	Scene 3	Scene 4	Scene 12	Scene 13
MME↓	PAloc	-8.65	-8.67	-8.34	-8.61	-8.74	-8.65
	FL2	-8.82	-8.76	-8.40	-8.69	-8.78	-8.78

[1] Smaller MME values are better; [2] Alg: algorithm; [3] FL2: FAST-LIO2; [4] Hu et al conducted a comparative analysis of MME in 14 scenes, but only in the above-listed scenes did FL2 perform better than PAloc.

In addition, the new LEMON-Mapping algorithm proposed by Wang et al. [35] in the paper in 2025 has an average MME entropy value of 0.07 lower in four scenes than the HBA (Hierarchical LiDAR Bundle Adjustment) algorithm. As shown in Table 3, we can see the specific MME data of Wang et al.

Table 3: Specific MME Data of Wang et al

Metrics	Alg.	Garage	Library	Yard	Laboratory
MME↓	HBA	-6.83	-5.95	-6.39	-6.26
	LEMON	-6.86	-6.23	-6.40	-6.20

1 Smaller MME values are better; 2 Alg: algorithm; 3 HBA: Hierarchical LiDAR Bundle Adjustment, LEMOM: LEMON-Mapping.
Special note: All data and tables in Section 3.1 have their sources noted and are not obtained by our experiments. Our experimental data are in Sections 3.3 and 3.4, as shown in Table 4.

3.2. Error map description

When performing MME metric calculation, MapEval will output the raw error map and inlier error map of the 3D point cloud map of the RTAB-Map algorithm and the 3D point cloud map of our framework. The main function of the raw error map is to color-code all points in the 3D point cloud map output by RTAB-Map. For each point in the 3D point cloud map output by RTAB-Map that does not find a corresponding point in the 3D point cloud map output by our framework, the default maximum error is 20cm, represented by red. On the other hand, the inlier error map excludes non-overlapping areas of the point cloud and only colors the errors of internal points after the point cloud is matched. Therefore, the inlier error map only contains a part of the points in the 3D point cloud map output by RTAB-Map.

3.3. Comparison results of each scene

3.3.1. Sparsely textured and empty rooms

RTAB-Map MME: - 8.38
Ours MME: -8.52
This scene lacks sufficient images and LiDAR feature points. We used the RTAB-Map algorithm and encountered drift problems in multiple mappings. After introducing our anti-interference module, the image contrast is improved, and the vision and laser odometry are more robust. The MME value dropped by 0.14. We can see from the error map in this scene that our loop closure detection effect is better than RTAB-Map, and ours is more robust in local map splicing. As shown in Figure 6, we can observe the mapping effect of scene 1 from the error map and MME map.

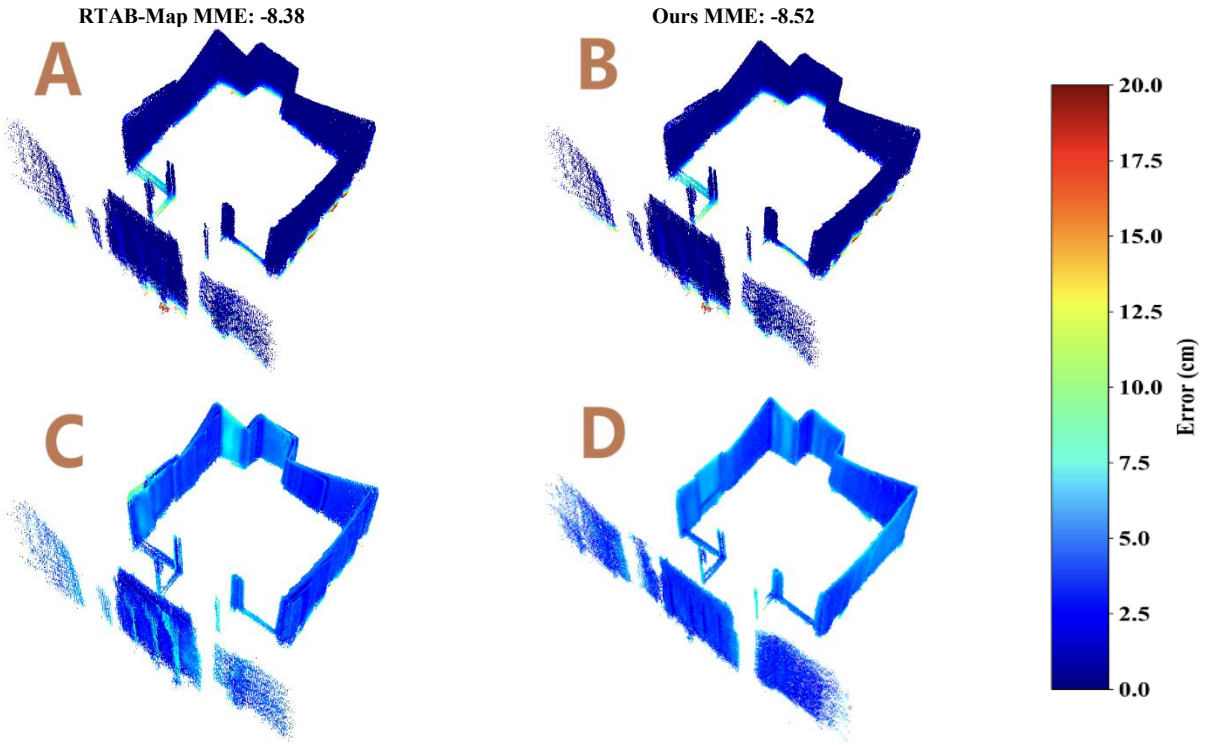

Fig. 6: (A) Scene 1 Raw Error Map. (B) Scene 1 Inlier Error Map. (C) Scene 1 RTAB-Map MME. (D) Scene 1: Our MME.

3.3.2. Sparsely textured and long corridors

RTAB-Map MME: -6.39
Ours MME: -6.47
In the corridor scene, the visual features are highly repetitive and far away. The original system repeatedly fails loop detection, and the system has significant drift and geometric ghosting. The enhanced module also improves the extraction of long-distance texture features in this scene. At the same time, the LiDAR filter effectively removes distant noise, improves the success rate of loop detection, and significantly improves map consistency. The MME value dropped by 0.08. We can see from the error map in this scene that our 3D point cloud is more regular than RTAB-Map, and ours has less drift and is more robust. As shown in Figure 7, we can observe the mapping effect of scene 2 from the error map and MME map.

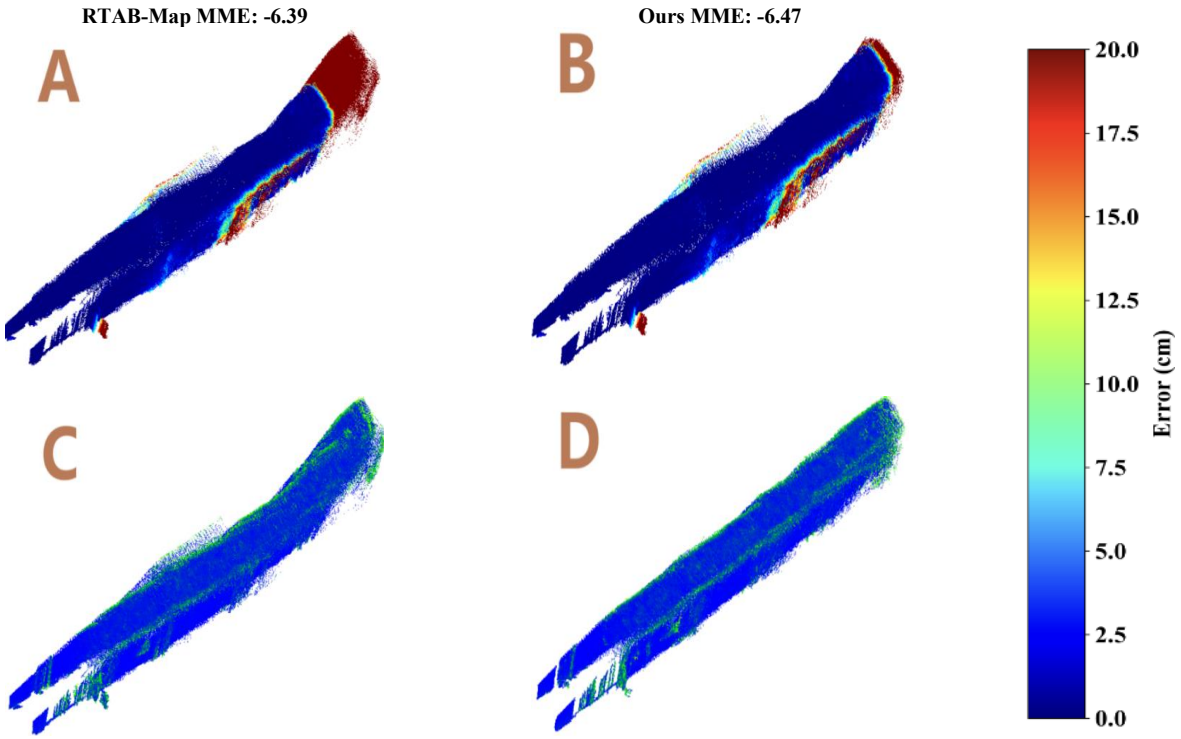

Fig. 7: (A) Scene 2 Raw Error Map. (B) Scene 2 Inlier Error Map. (C) Scene 2 RTAB-Map MME. (D) Scene 2 Our MME.

3.3.3. Sparsely textured and dimly lit stairwell

RTAB-Map MME: -6.58
Ours MME: -6.68
This scene is not well-lit, and the image lacks brightness and contrast. There are a few extractable feature points in the original image, the path drifts severely, and the map identity is extremely poor. CLAHE effectively enhances the brightness and contrast of handrails and stair edges, allowing the visual front end to extract stable features in dim light, ultimately forming a stable and continuous map. The MME value dropped by 0.10. We can see from the error map in this scene that our framework reduces interference, such as ghosting and blurring, when constructing local maps, which proves that our framework is more robust. As shown in Figure 8, we can observe the mapping effect of scene 3 from the error map and MME map.

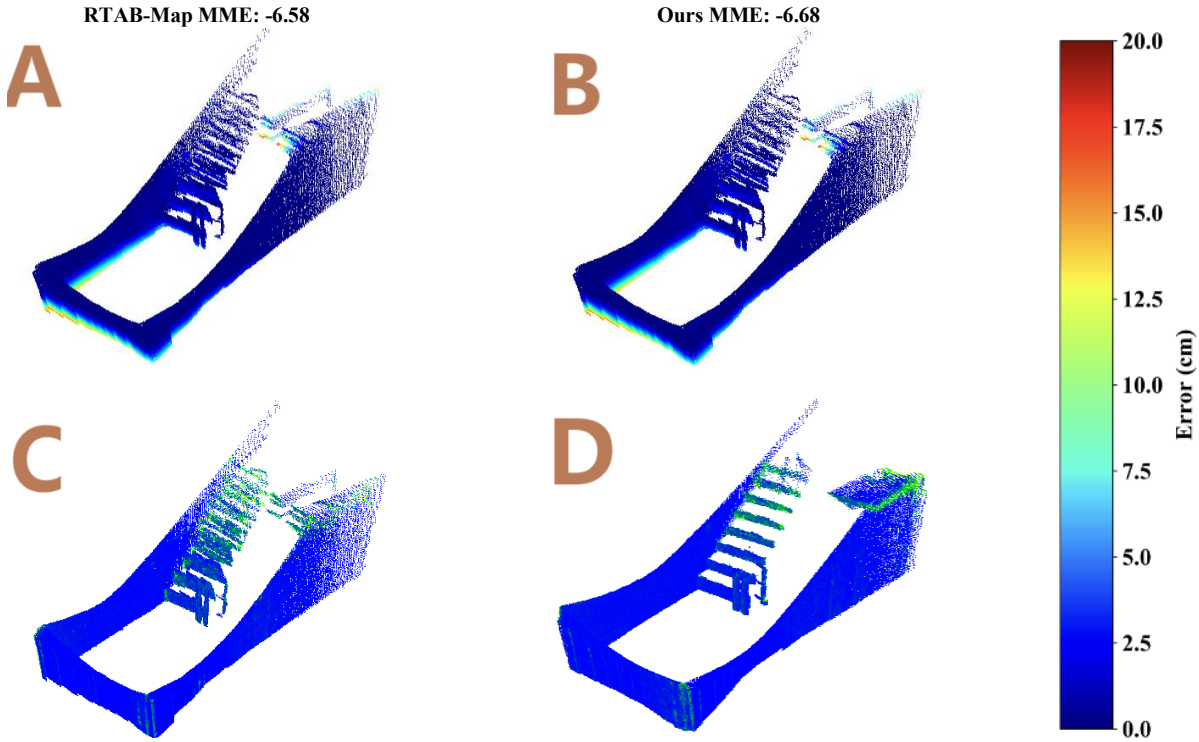

Fig. 8: (A) Scene 3 Raw Error Map. (B) Scene 3 Inlier Error Map. (C) Scene 3 RTAB-Map MME. (D) Scene 3: Our MME.

3.4. Average performance of experimental scenes

As shown in Figure 9, we can intuitively see the MME gap between RTAB-Map and our framework in three scenes. As shown in Table 4, we summarize the specific MME data obtained by RTAB-Map and our framework in three scenes.

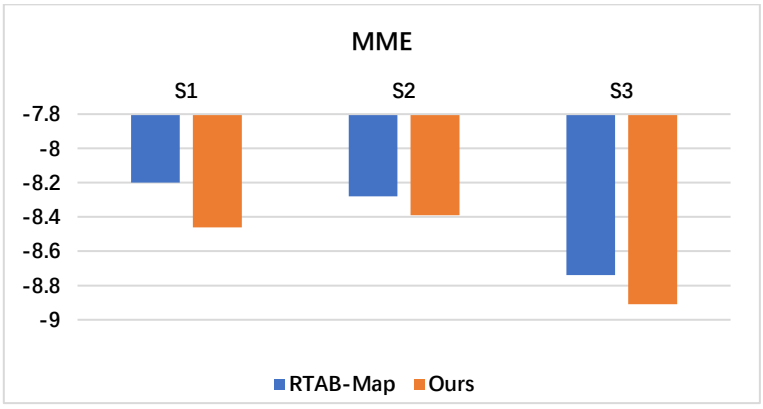

Fig. 9: Comparison of MME in three Scenes.

Table 4: MME Data of RTAB-Map and Our Framework in Three Scenes.

Metrics	Alg.	Scene1	Scene2	Scene3
MME↓	RTAB-Map	-8.38	-6.39	-6.58
	Ours	-8.52	-6.47	-6.68

1 Smaller MME values are better; 2 Alg: algorithm.

Our framework outperforms the original RTAB-Map algorithm in all three scenes. MME decreased by an average of 0.107 in the three environments. Especially in scene 1, an empty elevator room with sparse textures has the most significant improvement, and the MME value was 0.14 lower than the original algorithm, indicating that our framework has anti-interference ability in a perceptually degraded environment.

3.5. Discussion

3.5.1. Analysis of the advantages of our framework

From the experimental results, we can see that our framework has an improvement effect in some complex environments and performs well in solving the problem of visual and laser odometry degradation. The introduction of CLAHE improves the system's feature point extraction ability in scenes such as insufficient light and sparse texture, while the LiDAR Noise Filtering effectively removes abnormal point clouds, enhances the success rate of loop detection, and reduces local map mismatching. For real-world problems, our framework solves the drift problem in perception degradation scenes in a low-cost and lightweight way. For the scientific research community, compared with high-cost datasets, the research cost of our framework is lower.

3.5.2. Analysis of the disadvantages of our framework

Experimental results indicate that our framework currently has no significant side effects. However, in an environment with rich features and sufficient light, CLAHE may overexpose the image. The side effect of the LiDAR Noise Filtering is that when the LiDAR scans a slender object, it is easy to classify it as abnormal noise. Both of these situations are beyond the capabilities of our framework. CLAHE increases the probability of object recognition by enhancing contrast. In overexposure, where the image is completely lost, contrast adjustment cannot be used to increase image clarity. Therefore, we will need to introduce new algorithms, such as Gamma Correction, in future work. Similarly, LiDAR Noise Filtering module's misclassification occurs because the Median Deviation Filter misclassifies objects as noise after calculation. In other words, this situation is unavoidable as long as the Median Deviation Filter is used. Therefore, we may introduce new algorithms, such as the Neighborhood Search algorithm, in future work.

3.5.3. Impact on real-time performance

In our framework, the CLAHE module and the LiDAR Noise Filtering module are both run in node mode. We control the delay within 5ms, which has little impact on RTAB-Map. Our framework is relatively smooth when building maps, without key frame loss or serious map drift.

3.5.4. Verification of our framework's lightweight performance

To verify the lightweight nature of our framework, we use JTOP to record the average GPU usage of our framework under three perceptual degradation scenes, as shown in Table 5. Our framework can run on Jetson Orin Nano using about 60% of the computing power, while the original RTAB-Map algorithm uses about 43% of the computing power. Although our framework has increased its usage on Jetson Orin Nano by nearly 17%, we have also added the CLAHE module and LiDAR Noise Filtering module to RTAB-Map, which enables anti-interference and can run on the Jetson Orin Nano platform. In other words, we achieved anti-interference capabilities using 17% of the GPU's computing power, which is acceptable on the Jetson Orin Nano platform. Generally speaking, neural networks require an unacceptable amount of computing power and cannot be run on embedded platforms. So our framework is lightweight.

Table 5: GPU Usage of Jetson Orin Nano

Metrics	Alg.	Scene1	Scene2	Scene3
GPU Usage (%)	RTAB-Map	43%	45%	40%
	Ours	58%	61%	55%

4. Conclusions

4.1. Summary

We propose a framework to enhance the anti-interference ability of sensor data sources, which improves the robustness of the multi-sensor fusion SLAM system in the three perception degradation scenes of the above experiments to a certain extent. By introducing the CLAHE algorithm into visual data, the image feature extraction ability of the SLAM system in low-light environments is improved, and the LiDAR Noise Filtering module is designed to remove the abnormal LiDAR noise from far away, which effectively improves the mapping accuracy of the system in low-light, sparse texture, and LiDAR noise scenes. This paper completes field experiments in low-light, sparse texture, empty room, long straight corridor, and other environments on the physical vehicle platform. In the three scenes, the MME value was reduced by 0.14 at most and 0.107 on average.

4.2. Limitation analysis

Limited by the available experimental scenes, this paper does not cover all visual and LiDAR degradation scenes that may cause perception degradation, such as rain, fog, strong sunlight, etc., which have not been systematically tested and verified. Therefore, the scope of application of the current method needs to be expanded [36-40].

4.3. Future work

In future work, we will gradually cover common sensor perception degradation scenes and design targeted perception enhancement or compensation algorithms for each type of degradation. To address the shortcomings of this system, we will add an automatic weight adjustment system in future work. This system not only adjusts the credibility weights between sensor data, but also dynamically adjusts the parameters of each algorithm to adapt to different levels of perception degradation scenes. At the same time, we will try to improve the coordination between multi-sensor enhancement modules to enhance the system's mapping accuracy and positioning robustness in perception degradation scenes. The source code and dataset video for this study can be found at https://github.com/Ji-Yu887/A-novel-multi-sensor-fusion-SLAM-framework-for-anti-interference/tree/main

Acknowledgements

Author Contributions: "Conceptualization, Y.J. and J. Q.; methodology, Y.J. and J. Q.; software, Y.J. and J. Q.; validation, Y.J. and J. Q.; formal analysis, Y.J. and J. Q.; investigation, Y.J. and J. Q.; data curation, Y.J. and J. Q.; writing—original draft preparation, Y.J. and J. Q.; writing—review and editing, Y.J. and J.Q.; visualization, Y.J. and J. Q.; supervision, J. Q.; All authors have read and agreed to the published version of the manuscript."

Funding

The first author received scholarship support from CPALL for conducting this research in PIM.

Conflicts of interest

The authors declare no conflict of interest.

References

[1] Grisetti, G., Kummerle, R., Stachniss, C., & Burgard, W. (2010). A tutorial on graph-based SLAM. IEEE Intelligent Transportation Systems Magazine, 2(4). https://doi.org/10.1109/MITS.2010.939925.

[2] Liang, M., Yang, B., Chen, Y., Hu, R., & Urtasun, R. (2019). Multi-task multi-sensor fusion for 3D object detection. Proceedings of the IEEE Computer Society Conference on Computer Vision and Pattern Recognition, 2019-June. https://doi.org/10.1109/CVPR.2019.00752.

[3] Tang, Q., Liang, J., & Zhu, F. (2023). A comparative review on multi-modal sensors fusion based on deep learning. In Signal Processing (Vol. 213). https://doi.org/10.1016/j.sigpro.2023.109165.

[4] Liu, Z., Tang, H., Amini, A., Yang, X., Mao, H., Rus, D. L., & Han, S. (2023). BEVFusion: Multi-Task Multi-Sensor Fusion with Unified Bird's-Eye View Representation. Proceedings - IEEE International Conference on Robotics and Automation, 2023-May. https://doi.org/10.1109/ICRA48891.2023.10160968.

[5] Huang, Y., Shan, T., Chen, F., & Englot, B. (2022). DiSCo-SLAM: Distributed Scan Context-Enabled Multi-Robot LiDAR SLAM with Two-Stage Global-Local Graph Optimization. IEEE Robotics and Automation Letters, 7(2). https://doi.org/10.1109/LRA.2021.3138156.

[6] Labbé, M., & Michaud, F. (2019). RTAB-Map as an open-source lidar and visual simultaneous localization and mapping library for large-scale and long-term online operation. Journal of Field Robotics, 36(2). https://doi.org/10.1002/rob.21831.

[7] Phan, H. A., Nguyen, P. V., Khuat, T. H. T., Van, H. D., Tran, D. H. Q., Dang, B. L., Bui, T. T., Thanh, V. N. T., & Duc, T. C. (2023). A Sensor Fusion Approach for Improving Implementation Speed and Accuracy of RTAB-Map Algorithm Based Indoor 3D Mapping. Proceedings of JCSSE 2023 - 20th International Joint Conference on Computer Science and Software Engineering. https://doi.org/10.1109/JCSSE58229.2023.10201983.

[8] Yang, S., Song, Y., Kaess, M., & Scherer, S. (2016). Pop-up SLAM: Semantic monocular plane SLAM for low-texture environments. IEEE International Conference on Intelligent Robots and Systems, 2016-November. https://doi.org/10.1109/IROS.2016.7759204.

[9] Pire, T., Fischer, T., Castro, G., De Cristóforis, P., Civera, J., & Jacobo Berlles, J. (2017). S-PTAM: Stereo Parallel Tracking and Mapping. Robotics and Autonomous Systems, 93. https://doi.org/10.1016/j.robot.2017.03.019.

[10] Shan, T., Englot, B., Meyers, D., Wang, W., Ratti, C., & Rus, D. (2020). LIO-SAM: Tightly-coupled lidar inertial odometry via smoothing and mapping. IEEE International Conference on Intelligent Robots and Systems. https://doi.org/10.1109/IROS45743.2020.9341176.

[11] Tuna, T., Nubert, J., Nava, Y., Khattak, S., & Hutter, M. (2024). X-ICP: Localizability-Aware LiDAR Registration for Robust Localization in Extreme Environments. IEEE Transactions on Robotics, 40. https://doi.org/10.1109/TRO.2023.3335691.

[12] Xanthidis, M., Skaldebø, M., Haugaløkken, B., Evjemo, L., Alexis, K., & Kelasidi, E. (2024). ResiVis: A Holistic Underwater Motion Planning Approach for Robust Active Perception Under Uncertainties. IEEE Robotics and Automation Letters, 9(11), 9391–9398. https://doi.org/10.1109/LRA.2024.3455893.

[13] Chrysanthidis, G. (2023). lidar_noise_filtering. GitHub. https://github.com/ch-geo/lidar_noise_filtering (accessed 2025 05/03/2025).

[14] Yu, L., Yang, E., & Yang, B. (2022). AFE-ORB-SLAM: Robust Monocular VSLAM Based on Adaptive FAST Threshold and Image Enhancement for Complex Lighting Environments. Journal of Intelligent and Robotic Systems: Theory and Applications, 105(2). https://doi.org/10.1007/s10846-022-01645-w.

[15] Lin, X., Yang, X., Yao, W., Wang, X., Ma, X., & Ma, B. (2024). Graph-based adaptive weighted fusion SLAM using multimodal data in complex underground spaces. ISPRS Journal of Photogrammetry and Remote Sensing, 217, 101–119. https://doi.org/10.1016/j.isprsjprs.2024.08.007.

[16] Sabry, M., Osman, M., Hussein, A., Mehrez, M. W., Jeon, S., & Melek, W. (2022). A Generic Image Processing Pipeline for Enhancing Accuracy and Robustness of Visual Odometry. Sensors, 22(22). https://doi.org/10.3390/s22228967.

[17] Frosi, M., & Matteucci, M. (2022). ART-SLAM: Accurate Real-Time 6DoF LiDAR SLAM. IEEE Robotics and Automation Letters, 7(2), 2692–2699. https://doi.org/10.1109/LRA.2022.3144795.

[18] Ferrari, S., Giammarino, L. D., Brizi, L., & Grisetti, G. (2024). MAD-ICP: It is All About Matching Data – Robust and Informed LiDAR Odometry. IEEE Robotics and Automation Letters, 9(11), 9175–9182. https://doi.org/10.1109/LRA.2024.3456509.

[19] Li, M., & Mourikis, A. I. (2013). High-precision, consistent EKF-based visual-inertial odometry. The International Journal of Robotics Research, 32(6). https://doi.org/10.1177/0278364913481251.

[20] Lin, J., & Zhang, F. (2022). R3LIVE: A Robust, Real-time, RGB-colored, LiDAR-Inertial-Visual tightly-coupled state Estimation and mapping package. Proceedings - IEEE International Conference on Robotics and Automation. https://doi.org/10.1109/ICRA46639.2022.9811935.

[21] Jia, Y., Luo, H., Zhao, F., Jiang, G., Li, Y., Yan, J., Jiang, Z., & Wang, Z. (2021). Lvio-Fusion: A Self-adaptive Multi-sensor Fusion SLAM Framework Using Actor-critic Method. IEEE International Conference on Intelligent Robots and Systems. https://doi.org/10.1109/IROS51168.2021.9635905.

[22] Lee, J., Komatsu, R., Shinozaki, M., Kitajima, T., Asama, H., An, Q., & Yamashita, A. (2024). Switch-SLAM: Switching-Based LiDAR-Inertial-Visual SLAM for Degenerate Environments. IEEE Robotics and Automation Letters, 9(8), 7270–7277. https://doi.org/10.1109/LRA.2024.3421792.

[23] Li, Y., Zhang, W., Zhang, Z., Shi, X., Li, Z., Zhang, M., & Chi, W. (2025). An adaptive compensation strategy for sensors based on the degree of degradation. Biomimetic Intelligence and Robotics, 100235. https://doi.org/10.1016/j.birob.2025.100235.

[24] Hu, X., Wu, J., Jia, M., Yan, H., Jiang, Y., Jiang, B., Zhang, W., He, W., & Tan, P. (2025). MapEval: Towards Unified, Robust and Efficient SLAM Map Evaluation Framework. IEEE Robotics and Automation Letters, 10(5), 4228–4235. https://doi.org/10.1109/LRA.2025.3548441.

[25] Ding, S., & Qu, J. (2023). Research on Multi-tasking Smart Cars Based on Autonomous Driving Systems. SN Computer Science, 4(3), 292. https://doi.org/10.1007/s42979-023-01740-1.

[26] Li, Y., & Qu, J. (2024). A novel neural network architecture and cross-model transfer learning for multi-task autonomous driving. Data Technologies and Applications, 58(5), 693–717. https://doi.org/10.1108/DTA-08-2022-0307.

[27] Reke, M., Peter, D., Schulte-Tigges, J., Schiffer, S., Ferrein, A., Walter, T., & Matheis, D. (2020). A self-driving car architecture in ROS2. 2020 International SAUPEC/RobMech/PRASA Conference, SAUPEC/RobMech/PRASA 2020. https://doi.org/10.1109/SAUPEC/RobMech/PRASA48453.2020.9041020.
[28] Geneva, P., Eckenhoff, K., & Huang, G. (2018). Asynchronous Multi-Sensor Fusion for 3D Mapping and Localization. Proceedings - IEEE International Conference on Robotics and Automation. https://doi.org/10.1109/ICRA.2018.8460204.
[29] Eros, E., Dahl, M., Bengtsson, K., Hanna, A., & Falkman, P. (2019). A ROS2 based communication architecture for control in collaborative and intelligent automation systems. Procedia Manufacturing, 38. https://doi.org/10.1016/j.promfg.2020.01.045.
[30] Chen, K., Hoque, R., Dharmarajan, K., Llontopl, E., Adebola, S., Ichnowski, J., Kubiatowicz, J., & Goldberg, K. (2023). FogROS2-SGC: A ROS2 Cloud Robotics Platform for Secure Global Connectivity. IEEE International Conference on Intelligent Robots and Systems. https://doi.org/10.1109/IROS55552.2023.10341719.
[31] Patoliya, J., & Mewada, H. (2019). Comprehensive study and investigation of ROS for computer vision applications using Raspberry Pi. In International Journal of Engineering & Technology (Vol. 8, Issue 3). https://doi.org/10.14419/ijet.v8i3.29694.
[32] Bi, C., Shi, S., & Qu, J. (2024). Enhancing Autonomous Driving: A Novel Approach of Mixed Attack and Physical Defense Strategies. ASEAN Journal of Scientific and Technological Reports, 28(1), e254093. https://doi.org/10.55164/ajstr.v28i1.254093.
[33] Shi, S., & Qu, J. (2024). Multi-Task in Autonomous Driving through RDNet18-CA with LiSHTL-S Loss Function. ECTI Transactions on Computer and Information Technology, 18(2), 158–173.
[34] Hu, X., Zheng, L., Wu, J., Geng, R., Yu, Y., Wei, H., Tang, X., Wang, L., Jiao, J., & Liu, M. (2024). PALoc: Advancing SLAM Benchmarking With Prior-Assisted 6-DoF Trajectory Generation and Uncertainty Estimation. IEEE/ASME Transactions on Mechatronics, 29(6), 4297–4308. https://doi.org/10.1109/TMECH.2024.3362902.
[35] Wang, L.; Zhong, X.; Xu, Z.; Chai, K.; Zhao, A.; Zhao, T.; Jiang, C.; Wang, Q.; Zhang, F. (2025). LEMON-mapping: loop-enhanced large-scale multi-session point cloud merging and optimization for globally consistent mapping. arXiv, arXiv:2505.10018.
[36] Ding, S., & Qu, J. (2022). A Study on Safety Driving of Intelligent Vehicles Based on Attention Mechanisms. ECTI Transactions on Computer and Information Technology, 16(4). https://doi.org/10.37936/ecti-cit.2022164.248674.
[37] Gu, H., & Qu, J. (2025). Semantic-Aware Path Planning by Using Dynamic WeightedDijkstra for Autonomous Driving. International Journal of Basic and Applied Sciences, 14(3), 345-360. https://doi.org/10.14419/96xxwj87.
[38] Sizintsev, M., Rajvanshi, A., Chiu, H. P., Kaighn, K., Samarasekera, S., & Snyder, D. P. (2019). Multi-Sensor Fusion for Motion Estimation in Visually-Degraded Environments. 2019 IEEE International Symposium on Safety, Security, and Rescue Robotics, SSRR 2019. https://doi.org/10.1109/SSRR.2019.8848958.
[39] Tang, J., Liu, S., Liu, L., Yu, B., & Shi, W. (2020). LoPECS: A Low-Power Edge Computing System for Real-Time Autonomous Driving Services. IEEE Access, 8, 30467–30479. https://doi.org/10.1109/ACCESS.2020.2970728.
[40] Lu, G., Yang, H., Li, J., Kuang, Z., & Yang, R. (2023). A Lightweight Real-Time 3D LiDAR SLAM for Autonomous Vehicles in Large-Scale Urban Environment. IEEE Access, 11, 12594–12606. https://doi.org/10.1109/ACCESS.2023.3241800.